Theoretical and Applied Fracture Mechanics 97 (2018) 340–348

Contents lists available at ScienceDirect

Theoretical and Applied Fracture Mechanics

journal homepage: www.elsevier.com/locate/tafmec

Fatigue life assessment of notched round bars under multiaxial loading based on the total strain energy density approach

Ricardo Branco [a,*], J.D. Costa [a], Filippo Berto [b], F.V. Antunes [a]

[a] CEMMPRE, Department of Mechanical Engineering, University of Coimbra, Rua Luís Reis Santos, 3030-788 Coimbra, Portugal
[b] Department of Mechanical and Industrial Engineering, Norwegian University of Science and Technology, 7491 Trondheim, Norway

ARTICLE INFO

Article history:
Received 7 May 2017
Revised 31 May 2017
Accepted 2 June 2017
Available online 14 June 2017

Keywords:
Strain energy density
Notch effect
Notched round bars
U-shaped notches
Multi-axial loading
Fatigue life prediction

ABSTRACT

The main purpose of this paper is the fatigue assessment in lateral U-shaped notched round bars under bending-torsion loading. Despite its importance in the context of mechanical design, very little work has been done in this field. The fatigue life prediction model relies on the assumption that both the smooth and the notched samples fail when a critical value of the total strain energy density is reached. The *modus operandi*, in a first instance, consists of developing a fatigue master curve that relates the total strain energy density and the number of cycles to failure using smooth specimens subjected to strain-controlled conditions. In a second stage, the total strain energy density of the notched samples is computed from representative hysteresis loops obtained through a three-step procedure: reduction of the multiaxial stress state to an equivalent stress state using a linear-elastic finite-element model; definition of an effective stress range on the basis of the Theory of Critical Distances; and generation of a hysteresis loop applying the Equivalent Strain Energy Density concept in conjunction with the calculated effective stress range. The comparison between the experimental and the predicted lives has shown a very good correlation, with all points within a factor of 2.

1. Introduction

Most mechanical components with circular cross-sections contain notches because of design requirements. When subjected to multiaxial loading histories, the stress-strain responses at the geometric discontinuities may result in complex fatigue problems, even in cases of low plastic deformation. In this context, the full understanding of the notch effect is pivotal to develop safe and durable products. Moreover, due to the increasingly short product life cycles, lower batch sizes, and the growing need to reduce overall costs, products are developed in smaller time frames. Thus, the rapid assessment of fatigue life in notched members subjected to non-trivial loading scenarios is indispensable to increase efficiency and, ultimately, attain engineering excellence.

Fatigue life prediction models based on local approaches require detailed information about the stress-strain state at the notch root [1–6]. One of the most popular methods to deal with notch fatigue problems was formulated by Neuber [1], who stated that the geometric mean value of both the stress and strain concentration factors is constant at any load state, and equals the elastic stress concentration factor. Nevertheless, despite its popularity, strains at the notch root tend to be over-estimated [7]. Other popular methods are those based on the strain energy density [8]. Molski and Glinka [3] proposed the Equivalent Strain Energy Density (ESED) concept, which assumes that the strain energy density of the material in the yielded zone is virtually the same as the strain energy density assuming the material to be entirely elastic. Although in certain circumstances, it is more accurate than the above-mentioned method, notch root strains tend to be underestimated, when nominal stresses approach the yield stress [9]. A more general formulation, based on a fatigue master curve evaluated from the sum of the positive elastic and plastic strain energy densities of representative cyclic hysteresis loops, was suggested by Ellyin et al. [10,11]. Lazzarin et al. [6,12] developed a volume-based approach, in which the SED calculations are carried out in a material-related control volume. A recent literature review on strain energy density approaches can be found in Ref. [13].

The Theory of Critical Distances (TCD) is another successful group of methods capable of accounting for the notch effect on fatigue problems [14,15]. The different methods have in common the fact that the effective stresses at the fatigue process zone are defined on the basis of a characteristic material length, i.e. the well-known critical distance. The origin of this theory, introduced by Neuber, date back the middle of the last century [16]. In essence, the so-called Line Method (LM) states that the reference

* Corresponding author.
E-mail address: ricardo.branco@dem.uc.pt (R. Branco).

http://dx.doi.org/10.1016/j.tafmec.2017.06.003
0167-8442/

stress for fatigue assessment can be obtained by averaging the linear-elastic stress profile over a straight line emanating from the notch root. Some years later, Peterson [17] suggested that the reference stress could be computed from the linear-elastic stress profile at a given distance from the notch root, considerably simplifying the problem. This approach is known as the Point method (PM). An overview on different applications of the TCD to fatigue problems can be found elsewhere [18].

The benefit of assessing fatigue lives using local elasto-plastic stresses and strains from pseudo-elastic stresses in a practical perspective, i.e. simplicity, computational overhead, or overall costs, has encouraged new research on notch fatigue correction [19,20]. However, the above-mentioned approaches have some limitations. On the other hand, although fatigue life prediction models for uniaxial conditions are sufficiently mature, the same cannot be said for multiaxial loading. Furthermore, the identification of a universally accepted fatigue damage parameter has not been yet achieved [21,22]. Therefore, the development of reliable multiaxial fatigue life methodologies for notched components remains a challenging problem, and requires further research.

The present paper deals with the fatigue life prediction of notched round bars with lateral notches undergoing in-phase bending-torsion loading. Despite the relevance of lateral notched round bars in the context of mechanical design, few studies have been conducted so far [23–33]. It should likewise be noted that the existing research has been mainly focused on transverse circular holes, or circumferential notches. Lateral notches in round bars subjected to bending-torsion histories have not been sufficiently explored. The purpose of this study is to investigate this issue in greater depth. The paper starts with the description of the multiaxial fatigue life prediction model. Section 3 addresses the material employed, the low-cycle fatigue tests conducted to obtain the fatigue master curve, and the multiaxial fatigue test program of the notched specimens; as well as the linear-elastic finite-element model developed to compute the stress state at the notch. Section 4 analyses the total strain energy density of the smooth specimens; the loading effect on fatigue behaviour in the notched specimens; and ends with the comparison of the experimental and predicted fatigue lives. The last section presents the concluding remarks.

2. Fatigue life prediction model

The main steps of the fatigue life prediction model are schematised in Fig. 1. Basically, it assumes that both smooth and notched samples accumulate the same damage and have the same lives if the stress-strain histories at the initiation sites are identical; and that fatigue failure occurs when the total strain energy density defined as the sum of both the plastic and the positive elastic components at the initiation sites reaches a critical value.

The first step is devoted to the analysis of the stress-strain response of the material from smooth specimens under fully-reversed strain-controlled conditions. For each test, a hysteresis loop is selected, and the total strain energy density is evaluated. The information collected for various strain amplitudes enables the definition of a fatigue master curve in the form:

$$\Delta W_T = \kappa t (2N_f)^{\alpha t} + \Delta W_{0t} \quad (1)$$

where ΔW_T is the total strain energy density, κt and αt are constants, N_f is the number of cycles to failure, and ΔW_{0t} is the tensile elastic energy at the material fatigue limit. The fatigue master curve obtained in this step is represented in Fig. 1(d). The use of the positive elastic strain energy density makes this parameter sensitive to the mean stress effect [10,11].

With regard to the notched samples, the multiaxial stress states at the notch caused by different combinations of normal and shear stresses (see Fig. 1(a)) are reduced to uniaxial stress states through the computation of the von Mises equivalent stress range (Fig. 1 (b)). Then, this equivalent uniaxial stress state is averaged using the Line Method (LM) of the Theory of Critical Distances (TCD). The critical distance ($D_{LM} = 2a_0$) is defined from the El Haddad [34] parameter

$$a_0 = \frac{1}{\pi}\left(\frac{\Delta K_{th}}{\Delta \sigma_0}\right)^2 \quad (2)$$

where ΔK_{th} is the range of the threshold value of the stress intensity factor, and $\Delta\sigma_0$ is the fatigue limit of the unnotched specimen. Such constants are evaluated at the same stress ratio of the notched component to be assessed. After that, using the averaged von Mises stress range and the Equivalent Strain Energy Density concept [35], a representative hysteresis loop is generated (Fig. 1(c)). Finally, the total strain energy density of the hysteresis loop is inserted into the fatigue master curve (Eq. (1)) to estimate the fatigue life (Fig. 1(d)).

3. Experimental and numerical procedure

3.1. Material

This study was conducted using a DIN 34CrNiMo6 high strength steel, oil quenched and tempered (Q&T), supplied in the form of 20 mm-diameter bars. The production process comprised an austenitisation at 850–880 °C for approximately 30 min, followed by oil cooling and temper at about 660 °C for at least 2 h, and air cooling. Its main mechanical properties are summarised in Table 1.

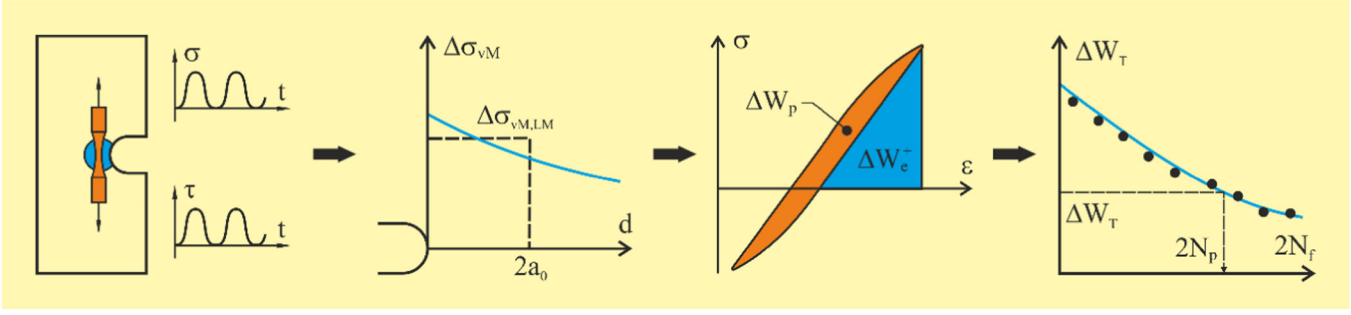

Fig. 1. Fatigue life prediction approach based on the total strain energy density evaluated at the initiation sites from hysteresis loops obtained through the ESED concept and an average stress given by the LM of the TCD: (a) reduction of the multiaxial stress state to an equivalent uniaxial stress state; (b) computation of the effective stress at the fatigue process zone; (c) calculation of the total strain energy density; (d) lifetime assessment using the fatigue master curve.

Table 1
Mechanical properties of the DIN 34CrNiMo6 high strength steel [32,36].

Yield strength, σ_{YS} [MPa]	967
Tensile strength, σ_{UTS} [MPa]	1035
Young's modulus, E [GPa]	209.8
Poisson's ratio, ν	0.296
Cyclic hardening coefficient, K′ [MPa]	1361.6
Cyclic hardening exponent, n′	0.1041
Fatigue limit stress range, $\Delta\sigma_0$ [MPa]	353
Stress intensity factor range threshold, ΔK_{th} [MPa·m$^{0.5}$]	7.12

3.2. Low-cycle fatigue tests of smooth specimens

Low-cycle fatigue tests were carried in a conventional servo-hydraulic machine, under fully-reversed strain-controlled conditions ($R_\varepsilon = -1$), for total strain amplitudes ($\Delta\varepsilon/2$) of 0.4, 0.5, 0.6, 0.8, 1.0, 1.25, 1.5, and 2.0% using a constant strain rate ($d\varepsilon/dt = 8 \times 10^{-3}\ s^{-1}$). Complementary, fully-reversed stress-controlled tests ($R_\sigma = -1$) with stress amplitudes ($\Delta\sigma/2$) of 540, 560, 580, 600, and 635 MPa were also performed. A more detailed description on the low-cycle fatigue behaviour of DIN 34CrNiMo 6 high strength steel can be found in Refs. [36,37].

The specimens were machined according to the specifications outlined in ASTM E606 with a gage section measuring 33.6 mm in length, and 8 mm in diameter. The final surface finishing was obtained by high-speed mechanical polishing using different grades of silicon carbide papers (P600-grit, P1200-grit, and P2500-grit) followed by 6-μm diamond paste.

The stress-strain response, during the tests, was acquired from a strain-gage extensometer mounted directly on the gage section connected to a digital data acquisition system. Tests were conducted using the single step method, and were interrupted when the specimens separated into two pieces.

3.3. In-phase bending-torsion fatigue tests of notched specimens

The fatigue test program of the notched specimens was conducted in a conventional servo-hydraulic machine connected to an own-made gripping system, at room temperature, under pulsating loading ($R \approx 0$), with frequencies at 3–6 Hz, and sinusoidal waveforms. More information on the fatigue test program and on the fatigue behaviour of DIN 34CrNiMo 6 high strength steel under bending-torsion can be found in Ref. [32].

The loading histories considered in this research were single bending, single torsion, and three different cases of combined bending-torsion, more specifically bending moment to torsion moment ratios (B/T) equal to 2, 1 and 2/3, which correspond to normal stress to shear stress (σ/τ) ratios equal to 4, 2 and 4/3, respectively. Three stress levels were considered for each case. A summary of the nominal normal and shear stresses applied in the test is presented in Table 2.

Fig. 2(a) and (b) shows the specimen geometries used in the experiments. The first one was used in the single bending and combined bending-torsion tests, while the other was used in the single torsion tests. Both geometries contained a U-shaped notch, placed asymmetrically with respect to the geometric centre of the specimen, with a diameter of 3 mm, and a depth of 3 mm. Before testing, the notch surfaces were polished with progressively finer grit papers (P600-grit, P1200-grit, and P2500-grit) followed by 6-μm diamond paste.

The detection of crack initiation and the observation of crack growth was carried out *in-situ* using a high-performance 14-bit charge-coupled device (CCD) digital camera with variable magnification. Images were recorded from a PC-based data acquisition system, on a periodic basis, i.e. every 5,000 cycles before crack detection, every 2,000 after crack detection, and every 1,000 in the final part of the test.

Table 2
Summary of the bending-torsion tests.

Specimen reference	Normal stress amplitude, σ_a [MPa]	Mean normal stress, σ_m [MPa]	Shear stress amplitude, τ_a [MPa]	Mean shear stress, τ_m [MPa]	Experimental life, N_i [cycles]	Predicted life, N_p [cycles]
Single bending						
B-1	197.4	208.1			65,765	119,169
B-2	197.4	208.1			135,085	119,169
B-3	218.8	229.3			53,742	77,221
B-4	219.3	228.5			37,108	77,221
B-5	288.6	297.6			10,675	16,761
B-6	288.6	297.6			16,956	16,761
Bending-torsion (B/T = 2): $\sigma_a = 4\tau_a$; $\sigma_m = 4\tau_m$; $\Delta\sigma = 4\Delta\tau$						
B2T-1	179.1	194.0	44.8	48.5	102,386	143,925
B2T-2	223.8	238.7	56.0	59.7	49,103	63,794
B2T-3	298.4	313.3	74.6	78.3	24,207	15,787
Bending-torsion (B/T = 1): $\sigma_a = 2\tau_a$; $\sigma_m = 2\tau_m$; $\Delta\sigma = 2\Delta\tau$						
BT-1	179.1	194.0	89.5	97.0	92,544	95,799
BT-2	179.1	194.0	89.5	97.0	83,278	95,799
BT-3	179.1	194.0	89.5	97.0	56,749	95,799
BT-4	223.8	238.7	111.9	119.4	26,420	37,653
BT-5	223.8	238.7	111.9	119.4	21,225	37,653
BT-6	223.8	238.7	111.9	119.4	31,306	37,653
BT-7	298.4	313.3	149.2	156.7	8314	8775
Bending-torsion (B/T = 2/3): $\sigma_a = 4/3\tau_a$; $\sigma_m = 4/3\tau_m$; $\Delta\sigma = 4/3\Delta\tau$						
B2T3-1	179.1	189.0	134.3	141.8	50,261	45,430
B2T3-2	223.8	233.8	167.9	175.3	17,967	14,654
B2T3-3	298.4	308.4	223.8	231.3	4099	3795
Single torsion						
T-1			167.1	178.2	108,731	126,360
T-2			167.1	178.2	171,230	126,360
T-3			200.5	211.6	56,636	64,483
T-4			200.5	211.6	42,941	64,483
T-5			222.8	233.7	29,291	39,997
T-6			245.0	256.1	25,190	24,810
T-7			245.0	256.1	36,424	24,810

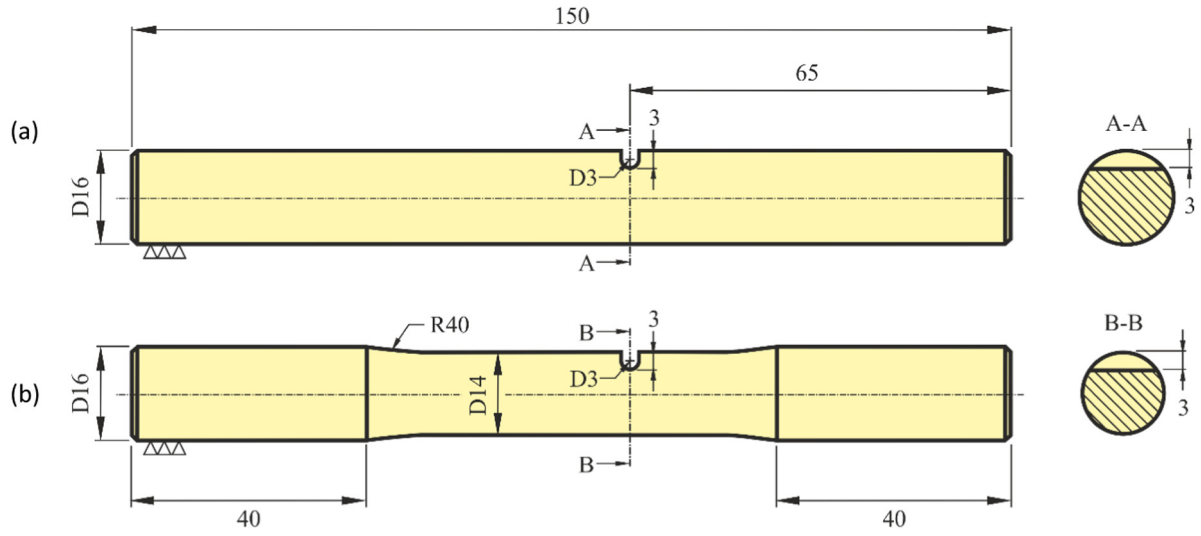

Fig. 2. Specimen geometries used in: (a) single bending and bending-torsion tests; and (b) single torsion tests (dimensions in millimetres).

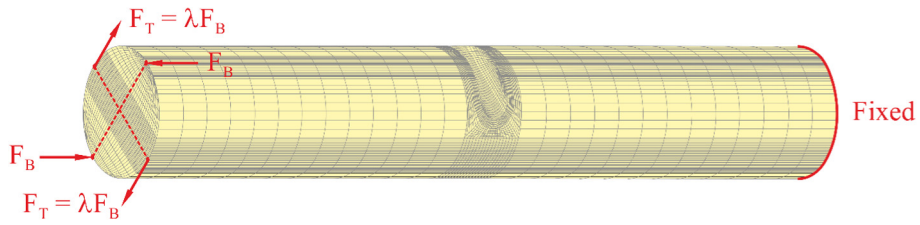

Fig. 3. Finite-element model developed in a parametric framework using 8-node hexahedrical isoparametric elements.

3.4. Finite-element model

Fig. 3 shows the finite-element model developed here to replicate the experimental tests. The mesh was created in a parametric framework, from 8-node isoparametric brick elements, with an ultra-refined region at the notch and a coarser one in the remaining volume of the body. The material was assumed linear-elastic, isotropic, and homogeneous. The assembled model contained 76,608 elements and 99,823 nodes.

The B/T ratios were defined by adjusting the relation between the bending and the torsion moments. The former and the latter moments were generated, respectively, by pairs of forces parallel (F_B) and normal (F_T) to the main axis of the specimen. The variable λ assumed, respectively, the value 1/2, 1, and 3/2 for the B/T ratio of 2, 1, and 2/3. The loads were applied at one end while the other was fixed. For the cases of single bending and single torsion only the forces F_B or F_T were applied, respectively.

4. Results and discussion

4.1. Total strain energy density of the smooth specimens

The cyclic stress-strain response of the material for various strain amplitudes, accounted for in terms of total strain energy density per cycle (ΔW_T) versus fatigue life ratio (N/N_f), is presented in Fig. 4. Here, as already mentioned, the total strain energy density per cycle (ΔW_T), is given by the sum of both the plastic strain energy (ΔW_P), and the positive elastic strain energy (ΔW_e^+). The material response, as can be seen in the figure, varies with the number of cycles. In a first stage, approximately equal to 10% of the life ratio, ΔW_T slightly decreases. Then, in a second stage, the total strain energy density remains practically constant up to life ratios of 95%. In the last part of the test, there is a rapid drop in ΔW_T until fatigue failure occurs. The ratio of the ΔW_T at the instant of failure to the ΔW_T at the half-life tends to raise for lower strain amplitudes. The value measured for $\Delta\varepsilon/2 = 2\%$ was only 84%, while for $\Delta\varepsilon/2 = 0.6\%$ the value increased to 98%.

Despite the variations observed in the initial and final stages, the total strain energy density is overall a very stable parameter. Based on this observation, the stabilised response of the material is defined from the half-life cycles obtained in the experiments. Fig. 5 shows representative hysteresis loops, obtained for various strain amplitudes, in a relative coordinate system, at which the maximum compressive stresses coincide at the origin. It is also plotted the cyclic curve, and the Masing curve (i.e. the cyclic curve magnified by a factor of two). Since the upper branches of the hysteresis loops are quite close to the Masing curve, an almost ideal Masing-type behaviour can be assumed for this material, as already reported in the literature [37].

The total strain energy density at the half-life versus the number of reversals to failure is exhibited in Fig. 6. The fitted function (Eq. (1)) is very well correlated with the experiments; the constants κt and αt, listed in Table 3, were calculated using the least square method. Fig. 6 also presents the plastic strain energy at the half-life against the number of reversals to failure. In a log-log scale, as can be seen, there is a linear correlation between both variables [11]. The measured values are quite close to those obtained by Sih et al. [38] using the isoenergy density theory. The total strain energy density, unlike for example the plastic

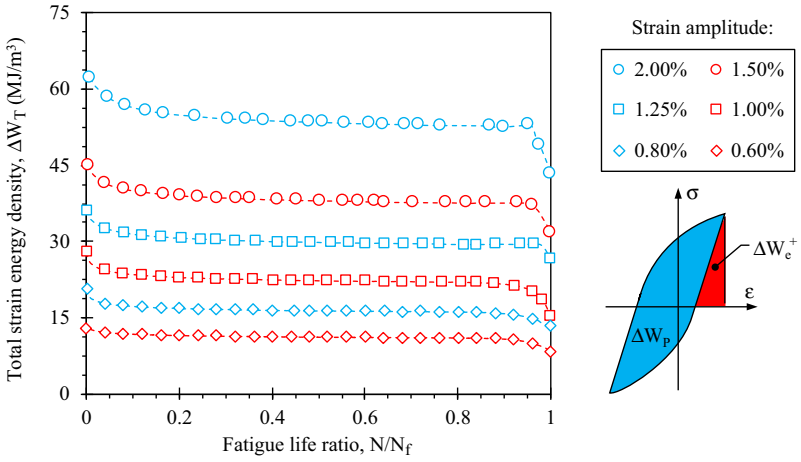

Fig. 4. Variation of the total strain energy density per cycle with the fatigue life ratio for various strain amplitudes for the DIN 34CrNiMo6 high-strength steel.

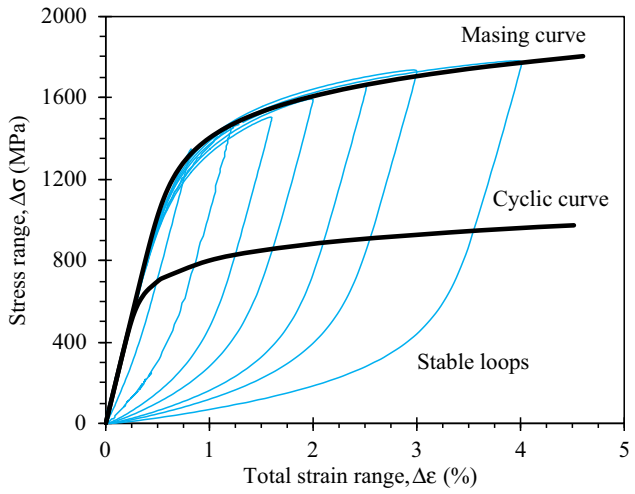

Fig. 5. Hysteresis loops at the half-life obtained for various strain amplitudes plotted in a relative coordinate system at which the maximum compressive stresses coincide for the DIN 34CrNiMo6 high-strength steel [37].

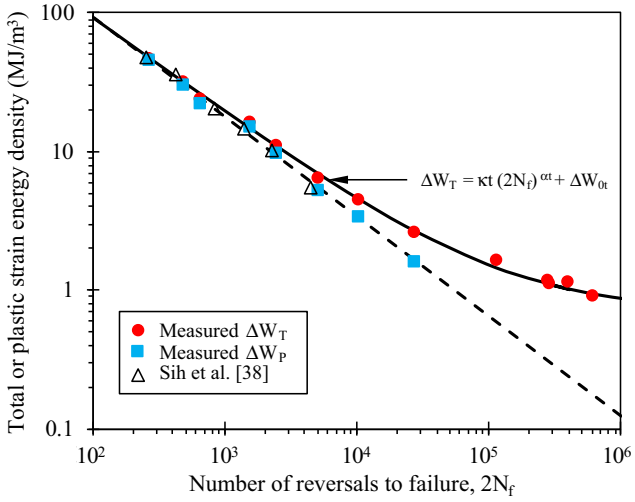

Fig. 6. Stable total and plastic strain energy densities at the half-life versus number of reversals to failure for the DIN 34CrNiMo6 high-strength steel determined from the fully-reversed strain-controlled tests [36].

Table 3
Constants of Eq. (1) obtained experimentally for DIN 34CrNiMo6 high strength steel [36].

Coefficient κt [MJ/m³]	Exponent αt	Constant ΔW₀t [MJ/m³]
2165.37	−0.6854	0.7049

strain energy, is able to unify both the low-cycle and high-cycle fatigue regimes, since ΔW_p cannot be accurately measured for longer lives, particularly close to the fatigue limit of the material [11]. In addition, as referred to above, the evaluation of the elastic energy associated with the tensile stress makes this parameter sensitive to the mean stress.

4.2. Experimental fatigue behaviour of the notched specimens

The crack paths at the notch surface, obtained in the experiments for the loading scenarios studied here, are displayed in Fig. 7. The crack paths, as expected, are significantly affected by the B/T ratio. In the absence of shear stress, as can be seen in Fig. 7(a), the crack grows in a plane normal to the longitudinal axis of the specimen, the so-called mode-I loading. The increase of the shear stress level becomes the crack path increasingly curved, resulting in out-of-plane propagation.

The experimentally detected initiation sites are shown in Fig. 7. The coloured circles correspond to the initiation sites of the samples exhibited in the figure; the white circles correspond to the initiation sites observed in the remaining samples; and the squares represent the numerical predictions. Predictably, there is a significant effect of the B/T ratio on the initiation sites. In Fig. 7(a), under single bending, the crack nucleates near the centre of the notch. For the other loading scenarios, due to the reduction of the σ/τ ratio, the defects tend to appear in positions closer to the curved edge of the notch. Furthermore, it can be concluded that the numerical predictions of the initiation sites, defined as the nodes of maximum first principal stress [32], are quite close to the experimental observations. The experimental observations have also shown, in most of the cases, the nucleation of the cracks from inclusions existing at the notch surface. The high susceptibility of this steel to the presence of non-metallic particles is well-documented in the literature [39,40]. A more detailed analysis of the effect B/T ratios on the crack paths, and the crack initiation sites can be found in Ref. [32].

Fatigue crack initiation lives were obtained from experimental relations between the surface crack length (2b) and the number

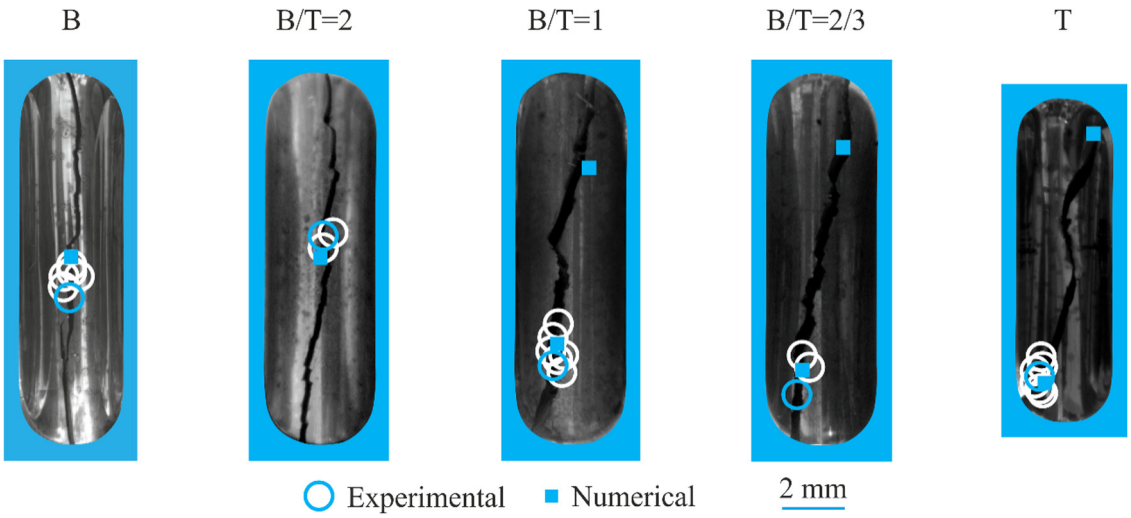

Fig. 7. Surface crack paths and initiation sites for different loading paths. Specimen reference: (a) B-1; (b) B2T-2; (c) BT2-1; (d) B2T3-2; (e) T-1.

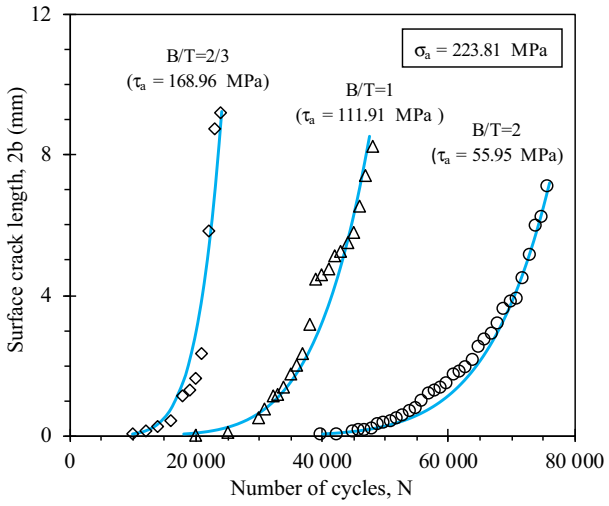

Fig. 8. Evolution of surface crack length with the number of cycles for different B/T ratios maintaining constant the nominal normal stress amplitude.

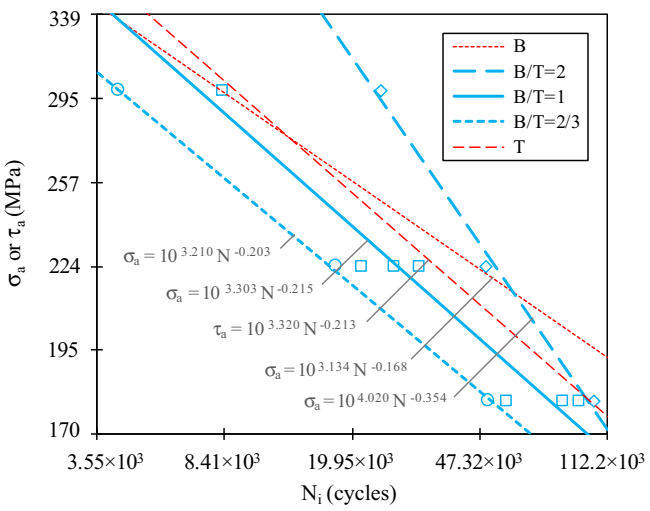

Fig. 9. S-N curves computed in terms of crack initiation lives and nominal normal or shear stress amplitudes for the various loading scenarios.

of cycles (N) or, in other words, from experimental 2b – N curves. Fig. 8 presents, as an example, three typical 2b – N curves obtained in the experiments for the same nominal normal stress amplitudes and three different B/T ratios. Not surprisingly, the higher is the nominal shear stress amplitude, the lower is the fatigue life. It is also clear from the figure that the slopes of the curves for the same crack length reduce with the B/T ratio. Overall, these trends were consistently observed in most of the tests, irrespective of the loading scenario [32].

The numbers of cycles to crack initiation (N_i), listed in Table 2, were originally calculated in reference [32]. Briefly, the procedure consists of calculating the crack initiation sizes through Eq. (2). For R = 0, the value of a_0 is equal to 123 μm. Then, the in-depth crack sizes (a_0) are related with the surface crack sizes ($2b_0$) using experimental values of crack aspect ratio (a_0/b_0) obtained from beach-marking tests performed for each loading scenario. According to Ref. [32], these ratios are approximately equal to 0.8. Therefore, for the same stress ratio, $2b_0$ = 308 μm. Using the value of $2b_0$, as well as the adequate 2b – N curve, the number of cycles to crack initiation is defined.

Fig. 9 shows, in a log-log scale, the so-called S-N curves computed in terms of crack initiation lives and nominal normal (or shear) stress amplitudes for the different loading cases studied here. For sake of clarity, only the fitted functions are displayed for single bending and single torsion. As expected, the slopes of the curves and the crack initiation lives are substantially different. In the multiaxial loading cases, both variables increase with the decrease of the shear stress level. Nevertheless, for higher lives, there seems to be a different trend in the series B/T = 2. However, it should be mentioned that this curve was fitted using a reduced number of specimens, only three. Therefore, it cannot be stated with absolute certainty.

4.3. Fatigue life prediction

The methodology proposed requires, in first instance, the reduction of the multiaxial stress state at the notch to an equivalent uniaxial stress state. This reduction is carried out by computing the von Mises equivalent stress range ($\Delta\sigma_{vM}$), at the initiation site, over a straight line emanating from the notch root. This computation is performed by using the linear-elastic finite-element model. The von Mises equivalent stress, as demonstrated in Ref. [32], is a very sensitive fatigue damage parameter, able to correlate the

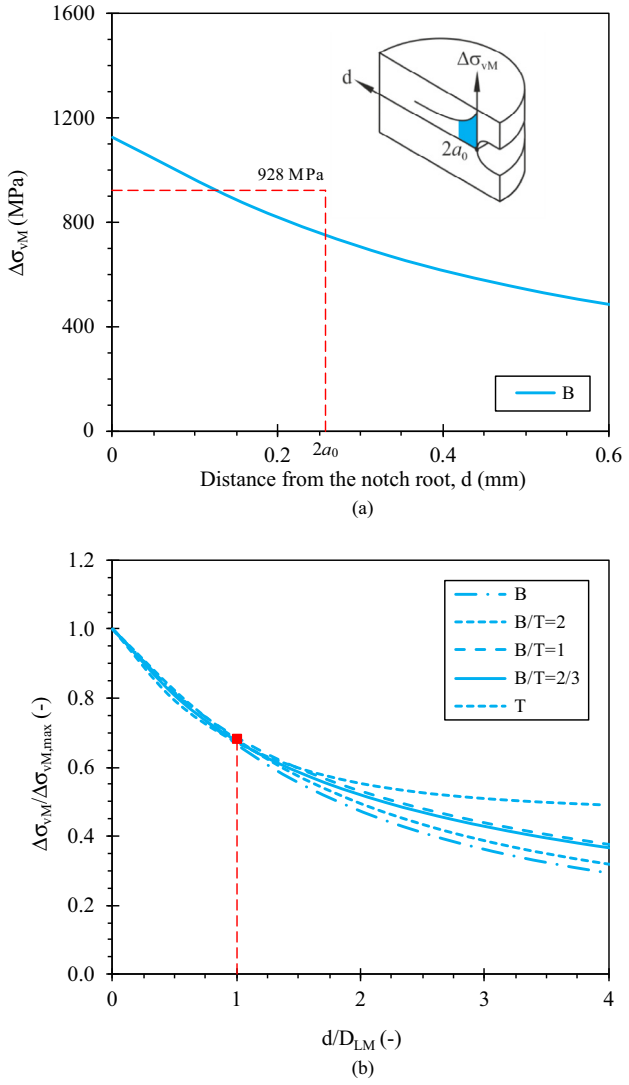

Fig. 10. Evolution of the local von Mises equivalent stress range with the distance from the notch root: (a) for a case of single bending; (b) in a dimensionless form for the different loading scenarios.

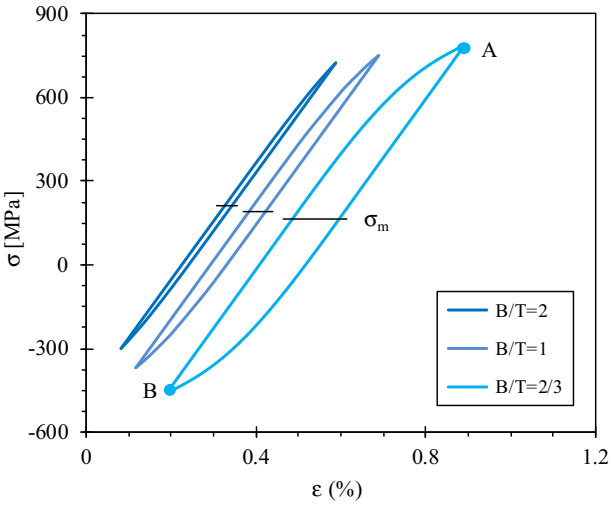

Fig. 11. Hysteresis loops obtained from the average stress using the ESED concept for three different B/T ratios under the same nominal normal stress amplitude (σ_a = 223.81 MPa).

stress state and the fatigue life for these loading conditions, and for these notch geometries. Fig. 10(a) displays the variation of $\Delta\sigma_{vM}$ at the initiation site over a straight line emanating from the notch root (d) for a case of single bending. Not surprisingly, the maximum elastic stress appears at the notch root and then decreases progressively to an asymptotical value.

Secondly, a reference stress is calculated by averaging the von Mises equivalent stress range over a critical distance ahead of the notch. Here, as referred to above, the average stress is determined using the LM of the TCD. In the case represented in Fig. 10 (a), the average stress is equal to 928 MPa. In Fig. 10(b), the elastic stress profiles for the various loading scenarios are compared in a dimensionless form, i.e. stresses are divided by the maximum value, and the distance from the notch root is divided by the critical distance ($D_{LM} = 2a_0$). Although the loading scenarios are substantially different as well as the initiation sites, it is interesting to note that the stress distributions in the critical region (i.e. values of d/D_{LM} lower than one) are basically overlapped. On the contrary, for higher distances, the dimensionless stress profiles follow different trajectories, and gradually move away from each other.

The next step is the generation of the hysteresis loops from the average stress ranges, which is done using the Equivalent Strain Energy Density concept [35]. Fig. 11 presents three stress-strain circuits obtained for identical nominal stress amplitudes but different B/T ratios (the three tests already represented in Fig. 8). The approach, as is well-known, starts with the calculation of both the maximum stress and the maximum strain (Point A). In a second stage, the stress range and the strain range are computed with respect to an auxiliary coordinate system with origin at Point A. This enables the definition of Point B. The amount of plastic strain, as can be concluded from the figure, clearly increases with the reduction of the B/T ratio or, in other words, due to the increase of the shear stress level. Therefore, predictably, fatigue lives tend to be smaller in such cases. This is consistent with the conclusions drawn from the results of Fig. 8. In fact, the reduction in fatigue life occurred for lower B/T ratios.

After that, the procedure consists of calculating the total strain energy density (ΔW_T) of each circuit. Finally, the fatigue lives are estimated by inserting the values of ΔW_T into Eq. (1). Fatigue life predictions (N_p) are listed in Table 2. Fig. 12 plots the predicted fatigue lives (N_P) against the experimental values (N_i). As can be

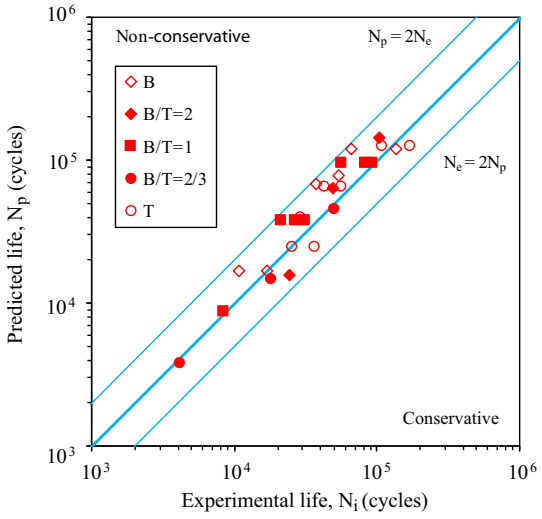

Fig. 12. Fatigue life predictions versus experimental fatigue lives obtained on the basis of the total strain energy density approach proposed here.

seen, there is a very good correlation, with 100% of the points within a factor of 2. Overall, as far as can be inferred, predictions tend to be non-conservative for single bending and for higher B/T ratios, and slightly conservative for single torsion and lower B/T ratios. Moreover, the analysis of fatigue lives shows that predictions tend to be conservative for values lower than 20×10^3 cycles, and non-conservative for higher numbers of cycles. To conclude, it should be highlighted that the current predictions considerably improve those presented in Ref. [32] which were done by combining the Coffin-Manson model and the ESED concept. Only 77% of the points were in the scatter bands.

5. Conclusions

This paper has addressed the fatigue life prediction in round bars with lateral notches under proportional bending-torsion loading. The model is based on the total strain energy density (ΔW_T) defined as the sum of the plastic and the positive elastic components. It assumes that both smooth and notched samples accumulate the same damage and have the same lives if the stress-strain histories at the initiation sites are identical; and that fatigue initiation occurs when a critical value of ΔW_T is reached.

The *modus operandi* consists of determining a fatigue master curve, defined in terms of total strain energy density versus number of cycles to failure. This material curve is defined from smooth specimens subjected to fully-reversed strain-controlled conditions. Then, a linear-elastic finite-element model is used to reduce the multiaxial stress state at the notch to an equivalent uniaxial stress state by accounting for the von Mises equivalent stress range at the initiation site. Then, with the Theory of Critical Distances, is computed an effective stress range. This effective stress range, in conjunction with the ESED concept, enables the generation of a representative hysteresis loop. Finally, the total strain energy density of this stress-strain circuit is compared with the fatigue master curve in order to estimate the fatigue life. The following conclusions can be drawn:

- The total strain energy density parameter is very stable throughout the entire life, and is characterised by an almost constant value. The half-life hysteresis loop is representative of the dissipated energy per cycle during the entire life.
- The reduction of the multiaxial stress state to an equivalent uniaxial stress state through the calculation of the local von Mises stress seems, in this case, to be sufficiently precise to correlate the fatigue life and the stress state.
- The very good correlation obtained between predicted and experimental lives shows that this approach can be efficiently used with U-shaped notched round bars undergoing in-phase bending-torsion loads.
- Although the fatigue life predictions have been slightly non-conservative for higher lives and, particularly, for cases of reduced level of shear stresses, all data have been inside scatter bands of 2.
- Predictions are carried from linear-elastic stresses, which enables a rapid evaluation of fatigue lives, provided that the material properties are known.

Acknowledgments

This research is sponsored by FEDER funds through the program COMPETE (under project T449508144-00019113) and by national funds through FCT – Portuguese Foundation for Science and Technology, under the project PTDC/EMS-PRO/1356/2014.

References

[1] H. Neuber, Theory of stress concentration for shear strained prismatical bodies with arbitrary non-linear stress-strain law, J. Appl. Mech. 28 (1961) 544–550.
[2] H.F. Hardrath, L. Ohman, A study of elastic and plastic stress concentration factors due to notches and fillets in fiat plates, NACA Report 117 (1953).
[3] K. Molski, G. Glinka, A method of elastic–plastic stress and strain calculation at a notch root, Mater. Sci. Eng. 50 (1981) 93–100.
[4] M. Hoffmann, T. Seeger, A generalized method for estimating elastic-plastic notch stresses and strains, J. Eng. Mater. Technol. 107 (1985) 250–260.
[5] F. Ellyin, D. Kujawski, Generalization of notch analysis and its extension to cyclic loading, Eng. Fract. Mech. 32 (1989) 819–826.
[6] P. Lazzarin, R. Zambardi, A finite-volume-energy based approach to predict the static and fatigue behaviour of components with sharp V-shaped notches, Int. J. Fract. 112 (2001) 275–298.
[7] J.D. Morrow, R.M. Wetzel, T.H. Topper, Laboratory simulation of structural fatigue behaviour, in': Effect of Environment and Complex Load History on Fatigue Life, American Society for Testing and Materials, ASTM STP462, Philadelphia, 1970, pp. 1–14.
[8] G.C. Sih, Strain-energy-density factor applied to mixed mode crack problems, Int. J. Fract. 10 (1974) 305–326.
[9] F. Ellyin, D. Kujawski, Notch root stress/strain prediction for elastic-plastic loading, Res. Mech. 20 (1987) 177–190.
[10] K. Golos, F. Ellyin, Generalization of cumulative damage criterion to multilevel cyclic loading, Theoret. Appl. Fract. Mech. 7 (1987) 169–176.
[11] F. Ellyin, Fatigue Damage, Crack Growth and Life Prediction, Chapman & Hall, London, 1997.
[12] P. Lazzarin, F. Berto, F.J. Gomez, M. Zappalorto, Some advantages derived from the use of the strain energy density over a control volume in fatigue strength assessments of welded joints, Int. J. Fatigue 30 (2008) 1345–1357.
[13] F. Berto, P. Lazzarin, A review of the volume-based strain energy density approach applied to V-notches and welded structures, Theoret. Appl. Fract. Mech. 52 (2009) 183–194.
[14] D. Taylor, Geometrical effects in fatigue: a unifying theoretical model, Int. J. Fatigue 21 (1999) 413–420.
[15] L. Susmel, D. Taylor, The theory of critical distances to estimate lifetime of notched components subjected to variable amplitude uniaxial fatigue loading, Int. J. Fatigue 33 (2011) 900–911.
[16] H. Neuber, Theory of Notch Stresses: Principles for Exact Calculation of Strength with Reference to Structural Form and Material, Springer, Berlin, Germany, 1958.
[17] R.E. Peterson, Notch sensitivity, in: G. Sines, J.L. Waisman (Eds.), Metal Fatigue, McGraw Hill, New York, 1958, pp. 293–306.
[18] L. Susmel, The theory of critical distances: a review of its applications in fatigue, Eng. Fract. Mech. 75 (2008) 1706–1724.
[19] V.B. Koettgen, M.E. Barkey, D.F. Socie, Pseudo stress and pseudo strain based approaches to multiaxial notch analysis, Fatigue Fract. Eng. Mater. Struct. 34 (2001) 854–867.
[20] A. Ince, G. Glinka, Innovative computational modeling of multiaxial fatigue analysis for notched components, Int. J. Fatigue 82 (2016) 134–145.
[21] A. Karolczuk, E. Macha, A review of critical plane orientations in multiaxial fatigue failure criteria of metallic materials, Int. J. Fract. 134 (1995) 267–304.
[22] B. Li, L. Reis, M. de Freitas, Comparative study of multiaxial damage models for ductile structural steels and brittle materials, Int. J. Fatigue 31 (2009) 1895–1906.
[23] P.H. Frith, Fatigue tests on crankshaft steels, J. Iron Steel Inst. 159 (1948) 385.
[24] H.J. Gough, Engineering steels under combined cyclic and static stresses, Inst. Mech. Eng. 160 (1949) 417–440.
[25] J.W. Fash, D.F. Socie, D.L. McDowell, Fatigue life estimates for a simple notched component under biaxial loading, in: K. Miller, M. Brown (Eds.), Multiaxial Fatigue, American Society for Testing and Materials, ASTM STP 853, 1985, pp. 497–513.
[26] S.M. Tipton, D.V. Nelson, Fatigue life predictions for a notched shaft in combined bending and torsion, in: K. Miller, M. Brown (Eds.), Multiaxial Fatigue, American Society for Testing and Materials, ASTM STP 853, 1985, pp. 514–50.
[27] P. Kurath, S.D. Downing, D.R. Galliart, Summary of non-hardened notched shaft round robin program, in: D. Socie, G. Leese (eds.), Multiaxial Fatigue: Analysis and Experiments, SAEAE-14. Society of Automotive Engineers, 1989, pp. 13–31.
[28] J. Park, D.V. Nelson, In-phase and out-of-phase combined bending-torsion fatigue of a notched specimen, in: S. Kalluri, P.J. Bonacuse (Eds.), Multiaxial Fatigue and Deformation: Testing and Prediction, ASTM STP 1387, American Society for Testing and Materials, ASTM STP1387, 2000, pp. 246–265.
[29] J.D. Costa, L.M.P. Abreu, A.C.M. Pinho, J.M. Ferreira, Fatigue behaviour of tubular AlMgSi welded specimens subjected to bending-torsion loading, Fatigue Fract. Eng. Mater. Struct. 28 (2005) 399–407.
[30] L. Abreu, J.D. Costa, J.M. Ferreira, Fatigue behaviour of AlMgSi tubular specimens subjected to bending-torsion loading, Int. J. Fatigue 31 (2009) 1327–1336.
[31] M. Firat, A numerical analysis of combined bending-torsion fatigue of SAE notched shaft, Finite Elem. Anal. Des. 54 (2012) 16–27.
[32] R. Branco, J.D. Costa, F.V. Antunes, Fatigue behaviour and life prediction of lateral notched round bars under bending-torsion loading, Eng. Fract. Mech. 119 (2014) 66–84.

[33] R. Branco, J.D. Costa, A. Veira, F. Berto, F.V. Antunes, Influence of loading ratio and loading orientation on fatigue behaviour in lateral notched round bars under bending-torsion, in: International Symposium on Notch Fracture, Santander, Cantabria, Spain, March 29–31, 2017.
[34] M.H. El Haddad, T.H. Topper, K.N. Smith, Prediction of non propagating cracks, Eng. Fract. Mech. 11 (1979) 573–584.
[35] G. Glinka, Calculation of inelastic notch-tip strain-stress histories under cyclic loading, Eng. Fract. Mech. 22 (1985) 839–854.
[36] R. Branco, J.D.M. Costa, F.V. Antunes, S. Perdigão, Monotonic and cyclic behavior of DIN 34CrNiMo6 tempered alloy steel, Metals 6 (2016) 98.
[37] R. Branco, J.D. Costa, F.V. Antunes, Low-cycle fatigue behaviour of 34CrNiMo6 high strength steel, Theor. Appl. Fract. Mech. 58 (2012) 28–34.
[38] G.C. Sih, D.Y. Jeong, Hysteresis loops predicted by isoenergy density theory for Polycrystals. Part II: cyclic heating and cooling effects predicted from nonequilibrium theory for 6061-T6 aluminum, SAE 4340 steel and Ti-8Al-1Mo-1V titanium cylindrical bars, Theoret. Appl. Fract. Mech. 41 (2004) 267–289.
[39] R. Barata, R.F. Martins, T. Albarran, T. Santos, A. Mourão, Failure analysis of a pull rod actuator of an ATOX raw mill used in the cement production process, Eng. Fail. Anal. 76 (2017) 99–114.
[40] J. Tartaglia, K. Lazzari, G. Hui, K. Hayrynen, A comparison of mechanical properties and hydrogen embrittlement resistance of austempered vs quenched and tempered 4340 steel, Metall. Mater. Trans. 39A (2008) 559–576.